Universal relations for hybridized *s*- and *p*-wave interactions from spin-orbital coupling

Fang Qin (覃昉) [1,2] and Pengfei Zhang [3,4,*]

[1]*Shenzhen Institute for Quantum Science and Engineering and Department of Physics,*
Southern University of Science and Technology (SUSTech), Shenzhen 518055, China
[2]*CAS Key Laboratory of Quantum Information, University of Science and Technology of China,*
Chinese Academy of Sciences, Hefei, Anhui 230026, China
[3]*Walter Burke Institute for Theoretical Physics, California Institute of Technology, Pasadena, California 91125, USA*
[4]*Institute for Quantum Information and Matter, California Institute of Technology, Pasadena, California 91125, USA*

In this work, we study the universal relations for one-dimensional spin-orbital-coupled fermions near both *s*- and *p*-wave resonances using effective field theory. Since the spin-orbital coupling mixes different partial waves, a contact matrix is introduced to capture the nontrivial correlation between dimers. We find the signature of the spin-orbital coupling appears at the leading order for the off-diagonal components of the momentum distribution matrix, which is proportional to $1/q^3$ (q is the relative momentum). We further derive the large frequency behavior of the Raman spectroscopy, which serves as an independent measurable quantity for contacts. Finally, we give an explicit example of contacts by considering a two-body problem.

I. INTRODUCTION

In ultracold-atomic gases, a series of universal relations was established to set up a bridge between the short-distance two-body correlations and the macroscopic thermodynamic properties [1–7]. These relations are connected by a set of key parameters called the contacts that have already been examined in experiments [8–12]. Later, the universal relations were also studied in higher partial-wave systems [13–18], low-dimensional systems [19–29], laser-dressed systems [30,31], and were taken into account in three-body correlations [32–36].

Recent experimental realization of the spin-orbital coupling (SOC) in ultracold gases [37–41] also leads to interesting few- and many-body physics [42–58]. In particular, the universal relations for the spin-orbital-coupled Fermi gases attract much attention [59–63]. Since the SOC breaks the rotational symmetry, it would mix different partial waves at the two-body level. It is interesting to study the universal relations for systems with one-dimensional (1D) SOC with both *s*- and *p*-wave interactions. Experimentally, a system with overlapping resonances of *s* and *p* waves has been realized in ^{40}K atoms using the optical control [64], where, in principle, additional SOC can be engineered directly.

Motivated by these developments, in this work, we study the universal relations for a 1D Fermi gas with hybridized *s*- and *p*-wave interactions from SOC. Importantly, we find that the q^{-3} tail in the spin-mixing (off-diagonal) terms of the momentum distribution matrix is a direct manifestation of the SOC-induced strong interplay of *s*- and *p*-wave interactions,

which can be observed through time-of-flight measurement. Further, we study the Raman spectroscopy and also find that the spin-mixing term of the Raman spectroscopy matrix is a useful experimental probe that can be used to detect the hybridization of *s*- and *p*-wave interactions. In the end, we calculate the contacts in two-body bound states as an explicit example of the contact matrix [65,66] in the hybridized *s*- and *p*-wave Fermi gases. It is found that there is a peak for the two-body hybridized contact of the *s* and *p* waves near the degenerate point of *s*- and *p*-wave scattering lengths, indicating a strong interplay between *s*- and *p*-wave dimers as expected.

The paper is organized as follows: In Sec. II, we give the model Hamiltonian and calculate the two-body physics. In Sec. III, we give the definition of the contacts. We calculate the large-momentum distribution tail in Sec. IV and we calculate the high-frequency tail of the Raman spectroscopy in Sec. V. In addition, we discuss other universal relations in Sec. VI. As a concrete example, we calculate the contacts in two-body states in Sec. VII. Finally, we provide a brief summary and discussions in Sec. VIII.

II. MODEL

The experiment [64] shows that the optical control of a *p*-wave magnetic Feshbach resonance can realize the noninteracting state between spin-down atoms near *s*-wave resonance, based on a laser-field-coupled bound-to-bound transition between the *p*-wave closed-channel molecular states. It can also be used to shift the *p*-wave Feshbach resonance associated with the spin-up atoms close to the resonance of the *s* wave in ^{40}K atoms. We consider a fermion system with an *s*-wave interaction between atoms with spin ↑ and ↓, together with a *p*-wave interaction between two spin-↑

*pengfeizhang.physics@gmail.com

fermions. Without SOC, the interesting few- and many-body physics have been studied in [67–71]. After adding the SOC, the effective 1D Lagrangian is given by ($\hbar = 1$ throughout the paper)

$$
\hat{L} = \sum_k \Psi_k^\dagger (i\partial_t - \mathcal{H}_k^0) \Psi_k
$$
$$
- \frac{g_S}{L} \sum_{Q,k,k'} \psi_{Q/2-k',\downarrow}^\dagger \psi_{Q/2+k',\uparrow}^\dagger \psi_{Q/2+k,\uparrow} \psi_{Q/2-k,\downarrow}
$$
$$
- \frac{g_P}{4L} \sum_{Q,k,k'} k' \psi_{Q/2-k',\uparrow}^\dagger \psi_{Q/2+k',\uparrow}^\dagger k \psi_{Q/2+k,\uparrow} \psi_{Q/2-k,\uparrow}, \tag{1}
$$

where L is the system size and g_S ($g_P/4$) is the effective 1D $s(p)$-wave coupling constant. We have defined $\Psi_k = (\psi_{k,\uparrow}, \psi_{k,\downarrow})^T$, where $\psi_{k,\sigma}$ is the field operator for the fermionic atoms with momentum k and spin σ. The single-particle Hamiltonian is $\mathcal{H}_k^0 = \frac{(kI_2+k_0\sigma_z)^2}{2m} + \Omega\sigma_x$, where atoms in the state $|\uparrow\rangle$ are coupled to the state $|\downarrow\rangle$ by the Raman laser with the strength Ω, and $2k_0$ is the momentum transfer during the two-photon processes. Here, $\sigma_{x/y/z}$ is the Pauli matrix and I_2 is the 2×2 identity matrix.

Before performing calculations, we would like to comment on the validity of the the Lagrangian (1). Similar to previous studies [72–74], the microscopic Hamiltonian in three dimensions can be divided into three parts: $H = H_0 + H_\perp + H_{\text{int}}$, where H_0 is the free Hamiltonian with SOC along the z direction, H_{int} is the three-dimensional (3D) interacting Hamiltonian with the 3D scattering parameters, and $H_\perp$ contains the transverse kinetic energy and transverse confinement potential. In real experiments, the trapping frequency of the transverse confinement potential is 10^5 Hz [75], which is much larger than a moderate SOC strength of $\sim 10^3$ Hz [38]. Since the length of the SOC is much longer than the potential range, i.e., the SOC in experiments [37–41] can barely reach the very short-range regime of the very deep short-range potential [51], the SOC will not modify the scattering inside the short-range potential. Consequently, when solving the scattering problem, we could separate the z coordinate into regions with $z \lesssim 1/\sqrt{\omega_\perp m}$ and $z \gtrsim 1/\sqrt{\omega_\perp m}$. In the region of $z \lesssim 1/\sqrt{\omega_\perp m}$, the problem is intrinsically 3D at high energy $\sim \omega_\perp$ and one could neglect both the kinetic energy in the z direction as well as the SOC. This gives the wave function at $z \sim 1/\sqrt{\omega_\perp m}$ up to leading order. The higher-order corrections are proportional to $E_z/(\omega_\perp m)$, which is sufficiently small compared with the leading-order term, where E_z can be the kinetic energy in the z direction or the SOC strength. The wave function for $z \gtrsim 1/\sqrt{\omega_\perp m}$ is determined by matching the boundary condition at $z \sim 1/\sqrt{\omega_\perp m}$, which can be modeled by a contact pseudopotential. Since, to the leading order, the boundary condition is determined by a Hamiltonian without SOC, there is no coupling between the s- and the p-wave contact pseudopotential, which leads to our Lagrangian (1). This analysis is consistent with the results presented in Refs. [72–74] when the transverse trapping frequency $\omega_\perp$ of the confinement potential is much larger than the strength of the SOC.

To conveniently calculate the Feynman diagrams, the above Lagrangian (1) can be rewritten as follows:

$$
\hat{L} = \sum_k \Psi_k^\dagger (i\partial_t - \mathcal{H}_k^0) \Psi_k + \sum_{Q;\alpha=S,P} \frac{\varphi_{Q,\alpha}^\dagger \varphi_{Q,\alpha}}{g_\alpha}
$$
$$
- \frac{1}{2\sqrt{L}} \sum_{Q,k} \left[\varphi_{Q,S}^\dagger (\Psi_{\frac{Q}{2}+k}^T \sigma_S \Psi_{\frac{Q}{2}-k}) + \text{H.c.} \right]
$$
$$
- \frac{1}{2\sqrt{L}} \sum_{Q,k} k \left[\varphi_{Q,P}^\dagger (\Psi_{\frac{Q}{2}+k}^T \sigma_P \Psi_{\frac{Q}{2}-k}) + \text{H.c.} \right], \tag{2}
$$

where we have used the definitions

$$
\varphi_{Q,S}^\dagger \equiv g_S \sum_{k'} \psi_{Q/2-k',\downarrow}^\dagger \psi_{Q/2+k',\uparrow}^\dagger / \sqrt{L}
$$

and

$$
\varphi_{Q,P}^\dagger \equiv \frac{1}{2} g_P \sum_{k'} k' \psi_{Q/2-k',\uparrow}^\dagger \psi_{Q/2+k',\uparrow}^\dagger / \sqrt{L}.
$$

$\varphi_{Q,S}$ ($\varphi_{Q,P}$) is the field operator of the $s(p)$-wave dimer with momentum Q. Note that although we have introduced a dimer field for convenience, the Lagrangian contains no dynamics of dimers and is essentially single channel. The generalization to two-channel models is straightforward and gives the same universal relations to the leading order. Interaction vertexes σ_S and σ_P can be related to Pauli matrices σ_j as $\sigma_S = i\sigma_y$, $\sigma_P = \frac{1}{2}(1 + \sigma_z)$, which is equivalent to

$$
\tfrac{1}{2} \Psi_{Q/2+k}^T \sigma_S \Psi_{Q/2-k} = \psi_{Q/2+k,\uparrow} \psi_{Q/2-k,\downarrow}, \tag{3}
$$

$$
\Psi_{Q/2+k}^T \sigma_P \Psi_{Q/2-k} = \psi_{Q/2+k,\uparrow} \psi_{Q/2-k,\uparrow}. \tag{4}
$$

To regularize the possible divergence, we impose a momentum cutoff at $k \sim \Lambda$. The bare interaction parameters g_S and g_P can be related to the physical scattering lengths by

$$
a_s = -\frac{2}{mg_S}, \quad \frac{1}{a_p} = \frac{4}{mg_P} + \frac{2\Lambda}{\pi}, \tag{5}
$$

where a_s (a_p) is the 1D $s(p)$-wave scattering length.

According to Eq. (5), g_S has unit of length^{-1} and g_P has unit of length. Moreover, since $\psi_\sigma(x) = \sum_k e^{ikx} \psi_{k,\sigma}/\sqrt{L}$, the dimension of $\psi_{k,\sigma}$ is length^0, knowing the dimension of $\psi_\sigma(x)$ is length$^{-1/2}$. In addition, $\sum_k \rightarrow L \int_{-\infty}^{\infty} dk/(2\pi)$ is dimensionless. Therefore, the unit of $\varphi_{Q,S}$ is length$^{-3/2}$ and the unit of $\varphi_{Q,P}$ is length$^{-1/2}$. $\varphi_{Q,S}$ and $\varphi_{Q,P}$ have different scaling dimensions and these quantities differ by a factor of length.

As mentioned before, we focus on a very special quasi-1D case where Ω and k_0^2 are much smaller than the transverse trapping frequency $\omega_\perp$ of the confinement potential, i.e., $\omega_\perp \gg \Omega$ and $\omega_\perp \gg k_0^2/m$. Consequently, in this limit, the scattering length would not depend on the SOC parameters, i.e., the reduction from 3D to 1D of the interaction receives no contribution from the SOC, consistent with the previous references [72–74]. In this case, the quasi-1D $s(p)$-wave scattering length connected to the three-dimensional (3D) one is given by [76–84]

$$
a_s = -\frac{\ell_\perp^2}{2a_{3D}} + \frac{\mathcal{C}\ell_\perp}{2}, \quad a_p = \frac{3V_p}{\ell_\perp^2}, \tag{6}
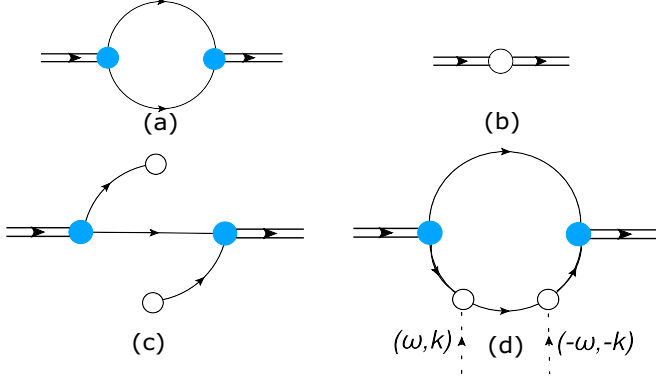$$

FIG. 1. (a) Diagrams for the matrix elements of the dimer-atom interaction operator. (b) Diagrams for the matrix elements of the dimer local operator $\varphi_\alpha^\dagger(R)\varphi_\beta(R)$ and its derivatives $\varphi_\alpha^\dagger(R)[i\partial_t + \partial_R^2/(4m)]^u(-i\partial_R)^v\varphi_\beta(R)$, with $u, v = 0, 1, 2, 3, \ldots$. (c) Diagram for the matrix elements of the operator $\psi_\sigma^\dagger(R + x)\psi_{\sigma'}(R)$. (d) Diagram for the matrix element of $\int dt\, e^{i\omega t - ikx} \int dx \mathcal{T} \mathcal{O}_{\sigma 3}(R + x, t) \mathcal{O}_{\sigma' 3}^\dagger(R, 0)$ ($\sigma = \uparrow, \downarrow$). The single line denotes the atom propagator matrix G, the double lines denote the matrix elements of the dimer propagator matrix $D_{\alpha\beta}$ with $\alpha, \beta \in \{S, P\}$, the blue dot represents the interaction vertex, $-i\sigma_\alpha$ or $-i\sigma_\beta$, and the open dot represents the insertion of operators.

where a_{3D} is the 3D s-wave scattering length, $\mathcal{C} = 1.4603$, $\ell_\perp = \sqrt{2/(m\omega_\perp)}$, $\omega_\perp$ is the transverse trapping frequency, and V_p is the 3D p-wave scattering volume.

With the above renormalization relation of g_P, the scattering amplitude of the model (2) is finite. Explicitly, the nontrivial part of the scattering amplitude is from the renormalization of the dimer Green's function $D_{\alpha\beta}(E_0, Q) = \langle \varphi_{Q,\alpha}(E_0)\varphi_{Q,\beta}^\dagger(E_0)\rangle$, where E_0 is the total energy. Here the expectation is under the real-time path integral with the Lagrangian (2). As shown in Fig. 1(a), the inverse of the dimer propagator matrix is given by

$$D^{-1}(E_0, Q)$$
$$= \begin{pmatrix} (ig_S)^{-1} - \Pi_{SS}(E_0, Q) & -\Pi_{SP}(E_0, Q) \\ -\Pi_{PS}(E_0, Q) & (ig_P)^{-1} - \Pi_{PP}(E_0, Q) \end{pmatrix},$$
$$(7)$$

where the polarization bubble reads

$$\Pi_{\alpha\beta}(E_0, Q) = -\int \frac{dp\, d\omega_0}{(2\pi)^2} \frac{p^{l_\alpha + l_\beta}}{2} \text{Tr}[G^T(\omega_0, Q/2 + p)\sigma_\alpha$$
$$\times G(E_0 - \omega_0, Q/2 - p)\sigma_\beta^\dagger],$$
$$(8)$$

where $\alpha, \beta \in \{S, P\}$ and we have defined $l_S = 0$ and $l_P = 1$. Tr denotes the trace over the spin degrees of freedom. G is the time-ordered Green's function matrix for fermions defined as $G_{\sigma\sigma'}(\omega, k) = \langle \psi_\sigma(\omega, k)\psi_{\sigma'}^\dagger(\omega, k)\rangle$. We have

$$[G^{-1}(\omega, k)]_{\sigma\sigma'} = -i[(\omega + i0^+)\delta_{\sigma\sigma'} - (\mathcal{H}_k^0)_{\sigma\sigma'}]. \quad (9)$$

The integral in (7) can be carried out analytically and we present the result with $Q = 0$ in the Supplemental Material [85]. Here, for simplicity, we only present the result for small

k_0 and Ω:

$$D^{-1}(E_0, 0) \approx \begin{pmatrix} -\frac{ma_s}{2} + \frac{m}{2\sqrt{-mE_0}} & \frac{\sqrt{m}k_0\Omega}{8(-E_0)^{3/2}} \\ \frac{\sqrt{m}k_0\Omega}{8(-E_0)^{3/2}} & \frac{m - a_p m\sqrt{-mE_0 + k_0^2}}{4a_p} \end{pmatrix}. \quad (10)$$

We have assumed $E_0 < 0$ and kept terms up to the k_0^2 and Ω order. The result shows that all divergence can be absorbed by the renormalization relation (5). In particular, the off-diagonal terms Π_{SP} and Π_{PS} are proportional to $k_0\Omega$ and thus finite, indicating the physics is universal. This is due to a nontrivial SOC, where we need both Ω and k_0 to be nonzero. In contrast, for the higher partial-wave systems in higher dimension, additional divergence may appear and new renormalization relations are needed.

III. CONTACT MATRIX

For a dilute atomic gas system described by (2), we expect universal behaviors governed by two-body physics when we focus on physics at some momentum scale k that satisfies $\Lambda \gg k \gg \max\{k_F, \sqrt{mT}\}$. Here, k_F is the Fermi momentum determined from the density of fermions and T is the temperature.

Theoretically, operator product expansion (OPE) is an ideal tool to explore such universal physics [4,5]. One can expand the product of two operators as

$$\mathcal{O}_i(x + R)\mathcal{O}_j(R)|_{x\to 0} = \sum_n C_{ij}^k(x)\mathcal{O}_k(R), \quad (11)$$

where $\{\mathcal{O}_i\}$ is a set of local operators and $C_{ij}^k(x)$ are expansion functions. After the Fourier transform, this gives the major contribution at large momentum. There is a similar expansion in time direction.

For a cold-atom system with only s- or p-wave interaction, it is known that the leading-order contribution is from the contact operator $\hat{C}_{SS}^{(0,0)}(R)$ or $\hat{C}_{PP}^{(0,0)}(R)$, which is given by Eq. (12). Intuitively, these contact operators count the effective number of dimers in a many-body system. When we turn on SOC, there is a finite correlation between the s- and p-wave dimers. We expect the system should instead be governed by the contact operator matrix,

$$\hat{C}_{\alpha\beta}^{(u,v)}(R) = m^{2+u}\varphi_\alpha^\dagger(R)\left(i\partial_t + \frac{\partial_R^2}{4m}\right)^u(-i\partial_R)^v\varphi_\beta(R), \quad (12)$$

where $u, v = 0, 1, 2, 3, \ldots$. The contact matrix of the system is then defined as $C_{\alpha\beta} = \int dR\langle \hat{C}_{\alpha\beta}(R)\rangle$. The idea of a matrix form contact was introduced in [65,66,86]. We now derive the universal relations for the momentum distribution and Raman spectral by matching their asymptotic behaviors with contact operators.

IV. MOMENTUM TAIL

Physically, we know that SOC should make spin $\uparrow$ and $\downarrow$ different. Hence, we consider the momentum distribution matrix $n_{\sigma'\sigma}(q) = \langle \psi_{q,\sigma}^\dagger \psi_{q,\sigma'}\rangle = \int dx dR e^{-iqx}\langle \psi_\sigma^\dagger(R + x)\psi_{\sigma'}(R)\rangle/L$, where q is the relative momentum. This corresponds to considering $\mathcal{O}_i = \psi_\sigma^\dagger$ and $\mathcal{O}_j = \psi_{\sigma'}$ in (11).

To determine the coefficient of OPE, we take the matrix elements for both sides of (11). Usually, one considers both

incoming and outgoing states with two fermions. However, in our model (2), two fermions can only interact by first combining to dimers and we could equivalently consider a single incoming dimer $|I_{\alpha_i}\rangle = \int dt\,dR\, e^{i(E_0 t - QR)}\varphi_{\alpha_i}^\dagger(R,t)|0\rangle$ and a single outgoing dimer $\langle O_{\alpha_o}| = \int dt\,dR\, e^{-i(E_0 t - QR)}\langle 0|\varphi_{\alpha_o}(R,t)$. Here, E_0 is the total energy and Q is the total momentum.

We first consider the matrix element of the contact operator matrix, which is expected to be the right-hand side of the OPE equation (11). The corresponding diagram is shown in Fig. 1(b):

$$\frac{C_{\alpha\beta}^{(u,v)}}{m^{2+u}} = \int dR \langle O_{\alpha_o}|\varphi_\alpha^\dagger(R,t)\left(i\partial_t + \frac{\partial_R^2}{4m}\right)^u$$
$$\times (-i\partial_R)^v \varphi_\beta(R,t)|I_{\alpha_i}\rangle$$
$$= \left(E_0 - \frac{Q^2}{4m}\right)^u \mathbf{Q}^v D_{\alpha_o\alpha}(E_0,Q)D_{\beta\alpha_i}(E_0,Q), \quad (13)$$

where E_0 is the total energy and $\mathbf{Q}$ is the total momentum. Notice that in one dimension, the momentum is still a vector

because a 1D vector has two opposite directions, and the 1D momentum can be defined as [87] $\mathbf{q} \equiv |q|\mathrm{sgn}(q)$, with the signum function $\mathrm{sgn}(q)$. Therefore, the quantity "bold Q" is defined as $\mathbf{Q} \equiv |Q|\mathrm{sgn}(Q)$, which means that the 1D center-of-mass momentum has two opposite directions. In this case, a vector or a scalar can be distinguished by their representation under inversion. If v is an odd number, the corresponding contact is a vector. This is to be matched with the matrix element of $\psi_\sigma^\dagger(R+x)\psi_{\sigma'}(R)$. The nontrivial interaction effect comes from the diagram shown in Fig. 1(c). After the Fourier transform, we get the momentum distribution matrix as

$$n(q) = \sum_{\alpha,\beta=S,P} (-i)^2 D_{\alpha_o\alpha}(E_0,Q)D_{\beta\alpha_i}(E_0,Q)\int_{-\infty}^{\infty}\frac{d\omega_0}{2\pi}q^{l_\alpha+l_\beta}$$
$$\times G(E_0-\omega_0,q)\sigma_\beta G^T(\omega_0,Q-q)\sigma_\alpha^\dagger G(E_0-\omega_0,q). \quad (14)$$

Keeping every element up to the order in the $1/q^4$ expansion, we have the momentum distribution matrix,

$$n(q) \sim \begin{pmatrix} \frac{C_{PP}}{q^2 L} + \frac{2\hat{\mathbf{q}}\cdot\mathbf{C}_{Q1}}{q^3 L} + \frac{2C_r - 2k_0^2 C_{PP} - 2k_0\hat{\mathbf{q}}\cdot\mathbf{C}_{Q1} + 5C_{Q2}/2}{q^4 L} + \frac{C_{SS}}{q^4 L} & -\frac{C_{SP}}{q^3 L} - \frac{2k_0 C_{SP} + 2\hat{\mathbf{q}}\cdot\mathbf{C}_{SPQ1}}{q^4 L} - \frac{m\Omega C_{PP}}{q^4 L} \\ -\frac{C_{PS}}{q^3 L} - \frac{2k_0 C_{PS} + 2\hat{\mathbf{q}}\cdot\mathbf{C}_{PSQ1}}{q^4 L} - \frac{m\Omega C_{PP}}{q^4 L} & \frac{C_{SS}}{q^4 L} \end{pmatrix}, \quad (15)$$

where $\sim$ means expanding to a certain order in the large-q limit, $\hat{\mathbf{q}} \equiv \mathbf{q}/|q|$ is the unit vector, and we use $C_{PP} = C_{PP}^{(0,0)}$, $\mathbf{C}_{Q1} = C_{PP}^{(0,1)}$, $C_r = C_{PP}^{(1,0)}$, $C_{Q2} = C_{PP}^{(0,2)}$, $C_{PS} = C_{PS}^{(0,0)}$, $C_{SP} = C_{SP}^{(0,0)}$, $\mathbf{C}_{PSQ1} = C_{PS}^{(0,1)}$, $\mathbf{C}_{SPQ1} = C_{SP}^{(0,1)}$, and $C_{SS} = C_{SS}^{(0,0)}$. Recall that the effective Lagrangian (2) is different from that in the laboratory frame by a momentum shift. For subleading terms, this momentum shift would modify the coefficient, as in [61,63]. However, the leading-order results in Eq. (15) are free from such complications. Moreover, note that this derivation can also be carried out for systems without SOC, which leads to the same leading-order results in Eq. (15). However, in that case, we have $C_{SP} = C_{PS} = 0$ due to the reflection symmetry. Here, the SOC plays a role of breaking the rotational symmetry and making C_{SP} and C_{PS} finite.

Experimentally, we could measure each component separately and extract their leading-order behaviors. As an example, for the off-diagonal terms, we could measure the momentum of fermions in the spin states $|\pm x\rangle = \frac{1}{\sqrt{2}}(|\uparrow\rangle \pm |\downarrow\rangle)$. Up to the leading order, this gives

$$n_{++}(q) - n_{--}(q) = n_{\downarrow\uparrow}(q) + n_{\uparrow\downarrow}(q) \sim -\frac{C_{PS}+C_{SP}}{q^3 L}.$$

Similarly, measuring in the spin states $|\pm y\rangle$ gives $C_{PS} - C_{SP}$.

V. RAMAN SPECTROSCOPY

The Raman spectroscopy can be used as an important experimental tool in cold-atom systems. When the transfer momentum and frequency are large, the Raman spectroscopy can also be related to the contacts. We consider applying a Raman coupling with frequency $\omega > 0$ and momentum k to transfers fermions from the internal spin state $|\sigma\rangle$ ($\sigma = \uparrow, \downarrow$) into a third spin state $|3\rangle$. The Hamilto-

nian reads $H_c = \sum_\sigma \Omega_\sigma \int dx\, e^{i(kx-\omega t)}\mathcal{O}_{\sigma 3}(x,t) + \mathrm{H.c.}$, where $\mathcal{O}_{\sigma 3}(x,t) \equiv \psi_3^\dagger(x,t)\psi_\sigma(x,t)$. The transition rate function $R(\omega,k)$ to $|3\rangle$ is given by the Fermi golden rule, which is related to the imaginary part of the time-ordered two-point correlation function [88,89]:

$$R(\omega,k) = 2\pi \sum_{\sigma\sigma'} \Omega_\sigma \Omega_{\sigma'}^* \Gamma_{\sigma\sigma'}^R(\omega,k), \quad (16)$$

$$\Gamma_{\sigma\sigma'}^R(\omega,k) = \frac{1}{\pi}\mathrm{Im}\int dR \int dt\, e^{i\omega t}\int dx\, e^{-ikx}$$
$$\times i\langle\mathcal{T}\mathcal{O}_{\sigma 3}(R+x,t)\mathcal{O}_{\sigma'3}^\dagger(R,0)\rangle, \quad (17)$$

where $\mathcal{T}$ is the time-ordering operator. We thus study the OPE of $\mathcal{O}_{\sigma 3}$ and $\mathcal{O}_{\sigma'3}^\dagger$. The diagram is shown in Fig. 1(d):

$$\Gamma_{\sigma\sigma'}^R(\omega,k)$$
$$= \frac{1}{\pi}\mathrm{Im}\, i \sum_{\alpha,\beta=S,P} (-i)^2 D_{\alpha_o\alpha}(E_0,Q)D_{\beta\alpha_i}(E_0,Q)$$
$$\times \int \frac{dp\,d\omega_0}{(2\pi)^2} p^{l_\alpha+l_\beta} G_0(E_0-\omega_0+\omega, p+k)$$
$$\times [G(E_0-\omega_0,p)\sigma_\beta^\dagger G^T(\omega_0,Q-p)\sigma_\alpha G(E_0-\omega_0,p)]_{\sigma\sigma'}. \quad (18)$$

Matching Eq. (18) with Eq. (13), we have the Raman transfer rate in the high-frequency and large-momentum limit,

$$\Gamma^R(\omega,k) = \frac{2m}{\pi\sqrt{4m\omega-k^2}}$$
$$\times \begin{pmatrix} \frac{2m\omega C_{PP}}{(k^2-2m\omega)^2} & \frac{k(k^2-6m\omega)C_{SP}}{(k^2-2m\omega)^3} \\ \frac{k(k^2-6m\omega)C_{PS}}{(k^2-2m\omega)^3} & \frac{2[4(m\omega)^2+4k^2 m\omega-k^4]C_{SS}}{(k^2-2m\omega)^4} \end{pmatrix}. \quad (19)$$

Here we have assumed $\omega > k^2/(4m)$ and kept each element to the leading order. Taking the limit of $k = 0$ leads to the high-frequency tail of the radio-frequency spectral $\Gamma^{\text{rf}}_{\sigma\sigma'}(\omega) = \Gamma^R_{\sigma\sigma'}(\omega, 0)$,

$$\Gamma^{\text{rf}}(\omega) = \frac{m}{2\pi} \begin{pmatrix} \frac{C_{PP}}{(m\omega)^{3/2}} & 0 \\ 0 & \frac{C_{SS}}{(m\omega)^{5/2}} \end{pmatrix}. \tag{20}$$

The result of $\Gamma^R(\omega, k)$ provides an individual experimental observable to determine different contacts by tuning Ω_σ (16). The Raman spectroscopy, together with the momentum distribution, serves as a nontrivial check for the universal relations in the hybridized system (2).

VI. OTHER UNIVERSAL RELATIONS

In this section, we discuss other universal relations, including the adiabatic relations and thermodynamical relations. Since the derivation is standard, we focus on presenting the results here and we give details of the derivations in the Supplemental Material [85].

We first focus on the adiabatic relations. The traditional s/p-wave contacts correspond to the change of energy when varying a_s or $-1/a_p$, which can be seen from taking the derivative with g_α in the Lagrangian (2) as

$$\frac{C_{SS}}{2m} \equiv \frac{\partial E}{\partial a_s}, \quad \frac{C_{PP}}{4m} \equiv -\frac{\partial E}{\partial a_p^{-1}}. \tag{21}$$

However, there is no direct s- and p-wave dimer mixing in (2) and thus no adiabatic relation for C_{SP} or C_{PS}. On the other hand, we could consider a nonspherical potential between atoms where microscopic mixing terms $\delta_{\text{SP}}\varphi^\dagger_{Q,S}\varphi_{Q,P}$ + H.c. exist in the action. In this case, the off-diagonal components of the contact matrix correspond to varying δ_{SP}.

When SOC is present, there are two new parameters k_0 and Ω. One can define two new contacts C_λ and C_Ω as

$$C_\lambda \equiv \frac{\partial E}{\partial k_0}, \quad C_\Omega \equiv \frac{\partial E}{\partial \Omega}. \tag{22}$$

Here, C_λ and C_Ω only refer to single-atom operators which give nonzero matrix elements in the single-atom sector. The momentum distribution under single-particle states is just

a delta function, so that C_λ and C_Ω will not contribute to the large-momentum tail, which is different from C_{SS} and C_{PP}. However, both k_0 and Ω have a nonzero energy scale, so that they would appear in the pressure relation and viral theorem. For a uniform gas, the pressure relation reads

$$\mathcal{P} = 2\mathcal{E} + \frac{a_s C_{SS}}{2mL} + \frac{C_{PP}}{4ma_pL} - \frac{k_0 C_\lambda}{L} - \frac{2\Omega C_\Omega}{L}, \tag{23}$$

where $\mathcal{E} = E/L$ is the energy density. For an atomic gas in a harmonic potential $V_T = m\omega^2 x^2/2$ with the trapping frequency ω, the viral theorem is written as

$$E = 2\langle V_T \rangle - \frac{a_s C_{SS}}{4m} - \frac{C_{PP}}{8ma_p} + \frac{k_0 C_\lambda}{2} + \Omega C_\Omega, \tag{24}$$

with $\langle V_T \rangle$ being the trapping energy.

VII. CONTACTS IN TWO-BODY BOUND STATES

To give an explicit example of the contact matrix in the hybridized s- and p-wave system, we now perform a calculation for the two-body bound state. Generally, the binding energy E_b with momentum Q is given by solving $\det[D^{-1}(E_0, Q)] = 0$. We consider the case with small SOC strength where we could use (10).

We focus on $Q = 0$ with both $a_s > 0$ and $a_p > 0$. For $\Omega = 0$, there is both an s-wave bound state with binding energy $E_b^{(s)} = -1/(ma_s^2)$ and a p-wave bound state with binding energy $E_b^{(p)} = -1/(ma_p^2) + k_0^2/m$. Here the presence of k_0 is because $Q = 0$ corresponds to a center-of-mass momentum $2k_0$ for the p-wave bound state in the laboratory frame. In this case, we have $C_{SS} = 4/a_s^3$, $C_{PP} = 8/a_p$, and $C_{SP} = C_{PS} = 0$.

When we turn on finite but small Ω, the binding energies receive an important correction only near the resonance with $1/(a_s^0)^2 = 1/(a_p^0)^2 - k_0^2$. We then approximate

$$D^{-1}(E_b, 0) \approx \begin{pmatrix} I_1\left(E_b - E_b^{(s)}\right) & K_\Omega \\ K_\Omega & I_2\left(E_b - E_b^{(p)}\right) \end{pmatrix}, \tag{25}$$

where $I_1 = \frac{m^2 a_s^3}{4}$, $I_2 = \frac{m^2 a_p}{8}$, and $K_\Omega = \frac{k_0 \Omega m^2 (a_s^0)^3}{8}$. Then the binding energy can be derived as

$$2E_b^{(\pm)} = E_b^{(p)} + E_b^{(s)} \pm \sqrt{\left(E_b^{(p)}\right)^2 - 2E_b^{(p)}E_b^{(s)} + \left(E_b^{(s)}\right)^2 + \frac{4K_\Omega^2}{I_1 I_2}}. \tag{26}$$

The contacts C_{SS} and C_{PP} can be derived by taking the derivation with a_s or $-1/a_p$. To calculate C_{SP} or C_{PS}, we apply the trick by adding the additional δ_{SP} terms and set them to be zero after taking derivatives.

The explicit formula for all contacts are given in the Supplemental Material [85]. A plot for $E_b^{(\pm)}$ and contacts for $E_b^{(-)}$ are shown in Figs. 2(a) and 2(c). Away from the degenerate point, $E_b^{(\pm)}$ approaches $E_b^{(s)}$ or $E_b^{(p)}$. Comparing Figs. 2(a)

with 2(c), it is found that the SOC parameters can open a gap between the two banding energies $E_b^{(+)}$ and $E_b^{(-)}$. Consequently, for the diagonal components of the contact matrix, we have $C_{SS} \approx 0$ for $a_s/a_p \gg 1$ and $C_{PP} \approx 0$ for $a_s/a_p \ll 1$. Near the degenerate point $a_s/a_p \sim 1$, we see a peak for C_{SP}, indicating a large mixing between s- and p-wave dimers as expected. Moreover, we also calculate the amplitude of the hybridized new contacts compared to the s- and p-wave ones
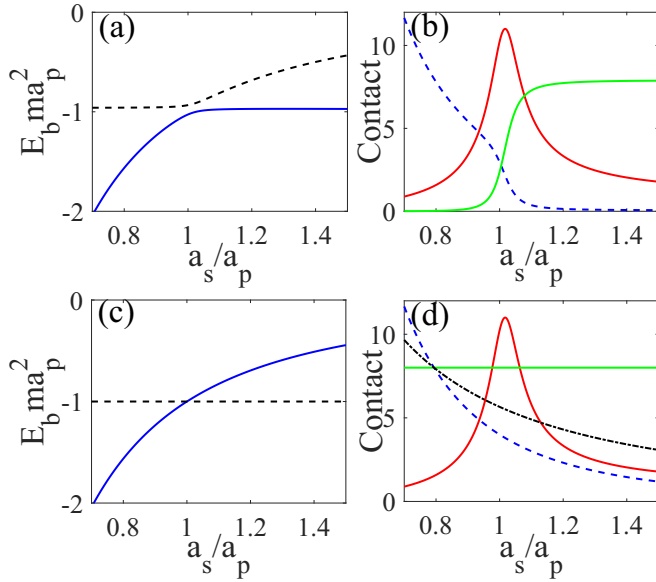
FIG. 2. (a) Dimensionless two-body banding energy vs a_s/a_p with SOC. The black dashed curve denotes $E_b^{(+)}ma_p^2$ and the blue solid curve denotes $E_b^{(-)}ma_p^2$. (b) Dimensionless two-body contacts vs a_s/a_p with SOC. (c) Dimensionless two-body banding energy vs a_s/a_p without SOC. The black dashed curve denotes $E_b^{(p)}ma_p^2$ and the blue solid curve denotes $E_b^{(s)}ma_p^2$. (d) Dimensionless two-body contacts C_{SS} and C_{PP} vs a_s/a_p without SOC. As a comparison, we also plot the C_{SP} with finite SOC [the same curve as (b)]. The red solid curve denotes $C_{SP}a_p^2$, the blue dashed curve denotes $C_{SS}a_p^3$, the green solid curve denotes $C_{PP}a_p$, and the black dot-dashed curve denotes $\sqrt{C_{SS}C_{PP}}a_p^2$. Here, we choose the SOC parameters as $k_0a_p = 0.2$ and $m\Omega a_p^2 = 0.3$.

without SOC, as shown in Fig. 2(d), to give the possibility of the measurement.

VIII. DISCUSSIONS

In this work, we have derived the momentum tail and the Raman spectroscopy for hybridized s- and p-wave interactions from spin-orbital coupling in 1D. We find new contacts appear at the leading order of certain observables due to the mixing between different partial waves.

We finally comment on the generalization to higher-dimensional systems with 1D (NIST) SOC. In higher dimensions, first, we have the additional quantum number $m = -1, 0, 1$ in 3D or $m = \pm 1$ in 2D for p-wave dimers. Depending on whether their resonance splits, we may have a larger contact matrix. To the leading order, the off-diagonal components of the momentum distribution should again correspond to the off-diagonal contacts and should be proportional to $1/q^3$. On the contrary, the scaling of the Raman spectral would change (by a factor of $\sim\omega^{(D-1)/2}$ for large ω) due to the difference of the density of state.

[1] S. Tan, Energetics of a strongly correlated Fermi gas, Ann. Phys. **323**, 2952 (2008).

[2] S. Tan, Large momentum part of a strongly correlated Fermi gas, Ann. Phys. **323**, 2971 (2008).

[3] S. Tan, Generalized virial theorem and pressure relation for a strongly correlated Fermi gas, Ann. Phys. **323**, 2987 (2008).

[4] E. Braaten and L. Platter, Exact Relations for a Strongly Interacting Fermi Gas From the Operator Product Expansion, Phys. Rev. Lett. **100**, 205301 (2008).

[5] E. Braaten, D. Kang, and L. Platter, Universal relations for a strongly interacting Fermi gas near a Feshbach resonance, Phys. Rev. A **78**, 053606 (2008).

[6] S. Zhang and A. J. Leggett, Universal properties of the ultracold Fermi gas, Phys. Rev. A **79**, 023601 (2009).

[7] S. B. Emmons, D. Kang, and L. Platter, Operator product expansion beyond leading order for two-component fermions, Phys. Rev. A **94**, 043615 (2016).

[8] J. T. Stewart, J. P. Gaebler, T. E. Drake, and D. S. Jin, Verification of Universal Relations in a Strongly Interacting Fermi Gas, Phys. Rev. Lett. **104**, 235301 (2010).

[9] Y. Sagi, T. E. Drake, R. Paudel, and D. S. Jin, Measurement Of The Homogeneous Contact Of A Unitary Fermi Gas, Phys. Rev. Lett. **109**, 220402 (2012).

[10] S. Hoinka, M. Lingham, K. Fenech, H. Hu, C. J. Vale, J. E. Drut, and S. Gandolfi, Precise Determination Of The Structure Factor And Contact In A Unitary Fermi Gas, Phys. Rev. Lett. **110**, 055305 (2013).

[11] C. Luciuk, S. Trotzky, S. Smale, Z. Yu, S. Zhang, and J. H. Thywissen, Evidence for universal relations describing a gas with p-wave interactions, Nat. Phys. **12**, 599 (2016).

[12] Bo. Song, Y. Yan, C. He, Z. Ren, Qi. Zhou, and G.-B. Jo, Evidence for bosonization in a three-dimensional gas of SU(N) fermions, arXiv:1912.12105.

[13] Z. Yu, J. H. Thywissen, and S. Zhang, Universal Relations For A Fermi Gas Close To A p-Wave Interaction Resonance, Phys. Rev. Lett. **115**, 135304 (2015).

[14] Z. Yu, J. H. Thywissen, and S. Zhang, Erratum: Universal Relations For A Fermi Gas Close To A p-Wave Interaction Resonance [Phys. Rev. Lett. **115**, 135304 (2015)], Phys. Rev. Lett. **117**, 019901(E) (2016).

[15] S. M. Yoshida and M. Ueda, Universal High-Momentum Asymptote And Thermodynamic Relations In A Spinless Fermi Gas With A Resonant p-Wave Interaction, Phys. Rev. Lett. **115**, 135303 (2015).

[16] M. He, S. Zhang, H. M. Chan, and Qi. Zhou, Concept Of A Contact Spectrum And Its Applications In Atomic Quantum Hall States, Phys. Rev. Lett. **116**, 045301 (2016).

[17] S.-G. Peng, X.-Ji. Liu, and H. Hu, Large-momentum distribution of a polarized Fermi gas and p-wave contacts, Phys. Rev. A **94**, 063651 (2016).

[18] P. Zhang, S. Zhang, and Z. Yu, Effective theory and universal relations for Fermi gases near a d-wave-interaction resonance, Phys. Rev. A **95**, 043609 (2017).

[19] M. Barth and W. Zwerger, Tan relations in one dimension, Ann. Phys. **326**, 2544 (2011).

[20] X. Cui, Universal one-dimensional atomic gases near odd-wave resonance, Phys. Rev. A **94**, 043636 (2016).

[21] X. Cui and H. Dong, High-momentum distribution with a subleading k^{-3} tail in odd-wave interacting one-dimensional Fermi gases, Phys. Rev. A **94**, 063650 (2016).

[22] O. I. Pâţu and A. Klümper, Universal tan relations for quantum gases in one dimension, Phys. Rev. A **96**, 063612 (2017).

[23] X. Yin, Xi.-W. Guan, Y. Zhang, H. Su, and S. Zhang, Momentum distribution and contacts of one-dimensional spinless Fermi gases with an attractive p-wave interaction, Phys. Rev. A **98**, 023605 (2018).

[24] M. Valiente, N. T. Zinner, and K. Mølmer, Universal relations for the two-dimensional spin-1/2 Fermi gas with contact interactions, Phys. Rev. A **84**, 063626 (2011).

[25] F. Werner and Y. Castin, General relations for quantum gases in two and three dimensions: Two-component fermions, Phys. Rev. A **86**, 013626 (2012).

[26] F. Werner and Y. Castin, General relations for quantum gases in two and three dimensions. II. Bsosons and mixtures, Phys. Rev. A **86**, 053633 (2012).

[27] J. Hofmann, Quantum Anomaly, Universal Relations, And Breathing Mode Of A Two-Dimensional Fermi Gas, Phys. Rev. Lett. **108**, 185303 (2012).

[28] Yi.-C. Zhang and S. Zhang, Strongly interacting p-wave Fermi gas in two dimensions: Universal relations and breathing mode, Phys. Rev. A **95**, 023603 (2017).

[29] S.-G. Peng, Universal relations for a spin-polarized Fermi gas in two dimensions, J. Phys. A: Math. Theor. **52**, 245302 (2019).

[30] F. Qin, J. Jie, W. Yi, and G.-C. Guo, High-momentum tail and universal relations of a Fermi gas near a Raman-dressed Feshbach resonance, Phys. Rev. A **97**, 033610 (2013).

[31] F. Qin, Universal relations and normal-state properties of a Fermi gas with laser-dressed mixed-partial-wave interactions, Phys. Rev. A **98**, 053621 (2018).

[32] E. Braaten, D. Kang, and L. Platter, Universal Relations For Identical Bosons From Three-Body Physics, Phys. Rev. Lett. **106**, 153005 (2011).

[33] D. H. Smith, E. Braaten, D. Kang, and L. Platter, Two-Body And Three-Body Contacts For Identical Bosons Near Unitarity, Phys. Rev. Lett. **112**, 110402 (2014).

[34] R. J. Fletcher, R. Lopes, J. Man, N. Navon, R. P. Smith, M. W. Zwierlein, and Z. Hadzibabic, Two- and three-body contacts in the unitary Bose gas, Science **355**, 377 (2017).

[35] P. Zhang and Z. Yu, Signature of the universal super Efimov effect: Three-body contact in two-dimensional Fermi gases, Phys. Rev. A **95**, 033611 (2017).

[36] P. Zhang and Z. Yu, Universal three-body bound states in mixed dimensions beyond the efimov paradigm, Phys. Rev. A **96**, 030702(R) (2017).

[37] Y.-J. Lin, K. Jimenez-Garcia, and I. B. Spielman, Spin-orbit-coupled Bose-Einstein condensates, Nature (London) **471**, 83 (2011).

[38] P. Wang, Z.-Q. Yu, Z. Fu, J. Miao, L. Huang, S. Chai, H. Zhai, and J. Zhang, Spin-Orbit Coupled Degenerate Fermi Gases, Phys. Rev. Lett. **109**, 095301 (2012).

[39] L. W. Cheuk, A. T. Sommer, Z. Hadzibabic, T. Yefsah, W. S. Bakr, and M. W. Zwierlein, Spin-Injection Spectroscopy Of A Spin-Orbit Coupled Fermi Gas, Phys. Rev. Lett. **109**, 095302 (2012).

[40] J.-Yi. Zhang, Si.-C. Ji, Z. Chen, L. Zhang, Z.-D. Du, Bo. Yan, Ge.-S. Pan, Bo. Zhao, Y.-J. Deng, H. Zhai, S. Chen, and J.-W. Pan, Collective Dipole Oscillations Of A Spin-Orbit Coupled Bose-Einstein Condensate, Phys. Rev. Lett. **109**, 115301 (2012).

[41] V. Galitski and I. B. Spielman, Spin–orbit coupling in quantum gases, Nature (London) **494**, 49 (2013).

[42] N. Goldman, G. Juzeliunas, P. Öhberg, and I. B. Spielman, Light-induced gauge fields for ultracold atoms, Rep. Prog. Phys. **77**, 126401 (2014).

[43] J. Zhang, H. Hu, X.-Ji. Liu, and H. Pu, Fermi gases with synthetic spin-orbit coupling, Annu. Rev. Cold Atoms Mol. **2**, 81 (2014).

[44] H. ZHAI, Spin-orbit coupled quantum gases, Int. J. Mod. Phys. B **26**, 1230001 (2012).

[45] H. Zhai, Degenerate quantum gases with spin-orbit coupling: A review, Rep. Prog. Phys. **78**, 026001 (2015).

[46] P. Zhang, L. Zhang, and Y. Deng, Modified Bethe-Peierls boundary condition for ultracold atoms with spin-orbit coupling, Phys. Rev. A **86**, 053608 (2012).

[47] L. Zhang, Y. Deng, and P. Zhang, Scattering and effective interactions of ultracold atoms with spin-orbit coupling, Phys. Rev. A **87**, 053626 (2013).

[48] Z. Yu, Short-range correlations in dilute atomic Fermi gases with spin-orbit coupling, Phys. Rev. A **85**, 042711 (2012).

[49] Y. Wu and Z. Yu, Short-range asymptotic behavior of the wave functions of interacting spin-1/2 fermionic atoms with spin-orbit coupling: A model study, Phys. Rev. A **87**, 032703 (2013).

[50] X. Cui, Mixed-partial-wave scattering with spin-orbit coupling and validity of pseudopotentials, Phys. Rev. A **85**, 022705 (2012).

[51] X. Cui, Multichannel molecular state and rectified short-range boundary condition for spin-orbit-coupled ultracold fermions near p-wave resonances, Phys. Rev. A **95**, 030701(R) (2017).

[52] L. Dong, L. Jiang, and H. Pu, Fulde-Ferrell pairing instability in spin-orbit coupled Fermi gas, New J. Phys. **15**, 075014 (2013).

[53] L. Dong, Lu. Zhou, B. Wu, B. Ramachandran, and H. Pu, Cavity-assisted dynamical spin-orbit coupling in cold atoms, Phys. Rev. A **89**, 011602(R) (2014).

[54] L. Dong, C. Zhu, and H. Pu, Photon-induced spin-orbit coupling in ultracold atoms inside optical cavity, Atoms **3**, 182 (2015).

[55] Y. Dong, L. Dong, M. Gong, and H. Pu, Dynamical phases in quenched spin-orbit-coupled degenerate Fermi gas, Nat. Commun. **6**, 6103 (2015).

[56] Y.-C. Zhang, Z.-W. Zhou, B. A. Malomed, and H. Pu, Stable Solitons In Three Dimensional Free Space Without The Ground State: Self-Trapped Bose-Einstein Condensates With Spin-Orbit Coupling, Phys. Rev. Lett. **115**, 253902 (2015).

[57] S.-S. Zhang, Wu.-M. Liu, and H. Pu, Itinerant chiral ferromagnetism in a trapped Rashba spin-orbit-coupled Fermi gas, Phys. Rev. A **93**, 043602 (2016).

[58] C. Zhu, L. Dong, and H. Pu, Harmonically trapped atoms with spin-orbit coupling, J. Phys. B: At., Mol. Opt. Phys. **49**, 145301 (2016).

[59] S.-G. Peng, C.-X. Zhang, S. Tan, and K. Jiang, Contact Theory For Spin-Orbit-Coupled Fermi Gases, Phys. Rev. Lett. **120**, 060408 (2018).

[60] J. Jie, R. Qi, and P. Zhang, Universal relations of an ultracold Fermi gas with arbitrary spin-orbit coupling, Phys. Rev. A **97**, 053602 (2018).

[61] P. Zhang and N. Sun, Universal relations for spin-orbit-coupled Fermi gas near an *s*-wave resonance, Phys. Rev. A **97**, 040701(R) (2018).

[62] C.-X. Zhang, S.-G. Peng, and K. Jiang, Universal relations for spin-orbit-coupled Fermi gases in two and three dimensions, Phys. Rev. A **101**, 043616 (2020).

[63] F. Qin, P. Zhang, and P.-Lu. Zhao, Large-momentum tail of one-dimensional Fermi gases with spin-orbit coupling, Phys. Rev. A **101**, 063619 (2020).

[64] P. Peng, R. Zhang, L. Huang, D. Li, Z. Meng, P. Wang, H. Zhai, P. Zhang, and J. Zhang, Universal feature in optical control of a *p*-wave Feshbach resonance, Phys. Rev. A **97**, 012702 (2018).

[65] S. M. Yoshida and M. Ueda, *p*-wave contact tensor: Universal properties of axisymmetry-broken *p*-wave Fermi gases, Phys. Rev. A **94**, 033611 (2016).

[66] S.-L. Zhang, M. He, and Qi. Zhou, Contact matrix in dilute quantum systems, Phys. Rev. A **95**, 062702 (2017).

[67] H. Hu, L. Pan, and S. Chen, Strongly interacting one-dimensional quantum gas mixtures with weak *p*-wave interactions, Phys. Rev. A **93**, 033636 (2016).

[68] L. Yang, X. Guan, and X. Cui, Engineering quantum magnetism in one-dimensional trapped fermi gases with *p*-wave interactions, Phys. Rev. A **93**, 051605(R) (2016).

[69] Y. Jiang, D. V. Kurlov, X.-W. Guan, F. Schreck, and G. V. Shlyapnikov, Itinerant ferromagnetism in one-dimensional two-component Fermi gases, Phys. Rev. A **94**, 011601(R) (2016).

[70] F. Qin, X. Cui, and W. Yi, Universal relations and normal phase of an ultracold Fermi gas with coexisting *s*- and *p*-wave interactions, Phys. Rev. A **94**, 063616 (2016).

[71] LiHong Zhou, W. Yi, and XiaoLing Cui, Fermion superfluid with hybridized *s*- and *p*-wave pairings, Sci. China: Phys., Mech. Astron. **60**, 127011 (2017).

[72] Yi.-C. Zhang, S.-W. Song, and Wu.-M. Liu, The confinement induced resonance in spin-orbit coupled cold atoms with Raman coupling, Sci. Rep. **4**, 4992 (2014).

[73] R. Zhang and W. Zhang, Effective Hamiltonians for quasi-one-dimensional Fermi gases with spin-orbit coupling, Phys. Rev. A **88**, 053605 (2013).

[74] Su.-Ju. Wang, Q. Guan, and D. Blume, *k*-matrix formulation of two-particle scattering in a waveguide in the presence of one-dimensional spin-orbit coupling, Phys. Rev. A **98**, 022708 (2018).

[75] Y.-an. Liao, A. S. C. Rittner, T. Paprotta, W. Li, G. B. Partridge, R. G. Hulet, S. K. Baur, and E. J. Mueller, Spin-imbalance in a one-dimensional Fermi gas, Nature (London) **467**, 567 (2010).

[76] M. Olshanii, Atomic Scattering In The Presence Of An External Confinement And A Gas Of Impenetrable Bosons, Phys. Rev. Lett. **81**, 938 (1998).

[77] T. Bergeman, M. G. Moore, and M. Olshanii, Atom-Atom Scattering Under Cylindrical Harmonic Confinement: Numerical And Analytic Studies Of The Confinement Induced Resonance, Phys. Rev. Lett. **91**, 163201 (2003).

[78] X. Cui, Quasi-one-dimensional atomic gases across wide and narrow confinement-induced resonances, Phys. Rev. A **86**, 012705 (2012).

[79] F. Qin, J.-S. Pan, Su. Wang, and G.-C. Guo, Width of the confinement-induced resonance in a quasi-one-dimensional trap with transverse anisotropy, Eur. Phys. J. D **71**, 304 (2017).

[80] B. E. Granger and D. Blume, Tuning The Interactions Of Spin-Polarized Fermions Using Quasi-One-Dimensional Confinement, Phys. Rev. Lett. **92**, 133202 (2004).

[81] L. Pricoupenko, Resonant Scattering Of Ultracold Atoms In Low Dimensions, Phys. Rev. Lett. **100**, 170404 (2008).

[82] S.-G. Peng, S. Tan, and K. Jiang, Manipulation Of *p*-Wave Scattering Of Cold Atoms In Low Dimensions Using The Magnetic Field Vector, Phys. Rev. Lett. **112**, 250401 (2014).

[83] D. V. Kurlov and G. V. Shlyapnikov, Two-body relaxation of spin-polarized fermions in reduced dimensionalities near a *p*-wave Feshbach resonance, Phys. Rev. A **95**, 032710 (2017).

[84] Ya.-T. Chang, R. Senaratne, D. Cavazos-Cavazos, and R. G. Hulet, Collisional loss of one-dimensional fermions near a *p*-wave Feshbach resonance, arXiv:2007.03723.

[85] See Supplemental Material at http://link.aps.org/supplemental/10.1103/PhysRevA.102.043321 for (i) explicit form of the dimer Green's function, (ii) other universal relations including the adiabatic relations, the pressure relation, and the viral theorem, and (iii) details of the two-body calculation.

[86] In particular, in [66], the authors have studied the possible mixing between different partial waves for general atomic systems in 3D without SOC.

[87] V. E. Barlette, M. M. Leite, and S. K. Adhikari, Quantum scattering in one dimension, Eur. J. Phys. **21**, 435 (2000).

[88] E. Braaten, D. Kang, and L. Platter, Short-Time Operator Product Expansion For rf Spectroscopy Of A Strongly Interacting Fermi Gas, Phys. Rev. Lett. **104**, 223004 (2010).

[89] J. Hofmann, Current response, structure factor and hydrodynamic quantities of a two- and three-dimensional fermi gas from the operator-product expansion, Phys. Rev. A **84**, 043603 (2011).